ACADEMIC PRESS

Available online at www.sciencedirect.com

SCIENCE DIRECT®

Journal of Computational Physics 186 (2003) 295–307

JOURNAL OF COMPUTATIONAL PHYSICS

www.elsevier.com/locate/jcp

Numerical investigation of flows in Czochralski crystal growth by an axisymmetric lattice Boltzmann method

Y. Peng [a], C. Shu [a,*], Y.T. Chew [a], J. Qiu [b]

[a] *Department of Mechanical Engineering, National University of Singapore, 10 Kent Ridge Crescent, Singapore 119260, Singapore*
[b] *Institute of Fluid Science, Tohoku University, Katahira 2-1-1, Aoba-ku, Sendai, Japan*

Received 14 October 2002; received in revised form 28 January 2003; accepted 30 January 2003

Abstract

An alternative new method called lattice Boltzmann method (LBM) is applied in this work to simulate the flows in Czochralski crystal growth, which is one of the widely used prototypical systems for melt-crystal growth. The standard LBM can only be used in Cartesian coordinate system and we extend it to be applicable to this axisymmetric thermal flow problem, avoiding the use of three-dimensional LBM on Cartesian coordinate system. The extension is based on the following idea. By inserting position and time dependent source terms into the evolution equation of standard LBM, the continuity and NS equations on the cylindrical coordinate system [1] can be recovered. Our extension is validated by its application to the benchmark problem suggested by Wheeler [2].

1. Introduction

The single crystals form the foundation of modern technology. They are needed for scientific appraisal of crystallography, topography and tensor properties of all crystalline materials. Basically, there are three major prototypical systems for melt-crystal growth, namely, Czochralski growth; vertical Bridgman growth; and floating-zone growth. Among them, the Czochralski technique has been widely used. The modeling and understanding of heat and mass transfer for this flow have become an important issue in the optimization of the Czochralski technique in order to grow more uniform and better-quality crystals.

The combination of natural convection due to thermal gradients between the crystal and crucible and forced convection due to rotation of the crystal and the crucible makes the problem very complex in terms of thermodynamics and hydrodynamics. Several numerical methods have been developed to simulate such crystal growth flow problems [3–9], which all solve the conventional NS equations. The discretization of the convection terms in NS equations is very important for the numerical simulation of

* Corresponding author. Fax: +65-779-1459.
E-mail address: mpeshuc@nus.edu.sg (C. Shu).

0021-9991/03/$ - see front matter
doi:10.1016/S0021-9991(03)00067-6

such flow and it is common to choose the second-order central difference scheme. However, with the increase of heat conduction or rotations of crystal and crucible, which is required in the Czochralski growth technique in order to grow larger with less imperfection crystals, the convection terms in the flow equations become dominant. This makes the second-order central difference scheme be unsuitable due to enhanced numerical instability. This problem has been reported by Xu et al. [9]. They found that the use of the central difference scheme failed to provide converged solution at high Grashof and Reynolds numbers. In order to improve the stability condition, low-order upwind scheme has to be used, but its high numerical diffusive properties may give rise to less accurate solution. Considering the discretization problem for the convection terms happened in conventional methods, we use a relatively new numerical technique called lattice Boltzmann method (LBM) [10] to simulate such kind of crystal growth problem. This method is based on the concepts from kinetic theory, but it does not simulate individual particle motion like particle-based methods such as Molecular Dynamics or Direct Simulation Monte Carlo. Although detailed particle simulations can recover NS behavior in the continuum limit, they are too expensive to use. On the contrary, LBM can also recover NS behavior but it incorporates a simpler, probabilistic model of particle motion. This makes it much easier to compute. The kinetic nature of LBM introduces some important features that distinguish it from other conventional numerical methods. One of these is that the convection operator of LBM in phase space is linear, which will be shown in the following section. So there is no need to do any discretization for this convection term and the above-mentioned discretization difficulty for the convection terms can be avoided.

As we know, the standard LBM is based on the Cartesian coordinate system and has the essential restriction on the lattice uniformity, since all the lattice models are defined on the Cartesian coordinates and the standard LBM will recover the continuity and NS equations in the Cartesian coordinate system by Chapman–Enskog expansion. This will be described in the following section. However, Czochralski crystal growth is an axisymmetric flow which is a quasi-three-dimensional problem for the conventional NS solvers in the cylindrical coordinate system, since there is no change for any variable in the azimuthal direction. If we use the standard LBM, we can only use the Cartesian coordinate system to solve such kind of cylindrical flow problems, which means that we have to use the three-dimensional lattice model to solve the real three-dimensional problems, which complicate the problem as compared with the conventional NS solvers. In order to avoid such complication, we propose a new LBM scheme, which inserts the position and time dependent source terms into the evolution equation of the standard LBM, and makes it recover the continuity and NS equations on the cylindrical coordinate system by Chapman–Enskog expansion. This new scheme is based on the idea proposed by Halliday et al. [1] in 2001, and it has the following good features. Like conventional CFD solvers, it solves the quasi-three-dimensional problem instead of the real three-dimensional problem for an axisymmetric flow. At the same time, it is applied on a uniform rectangular grid in the cylindrical coordinate system, which adheres to the inherit property of LBM. The curved boundary can also be well defined using the uniform rectangular grid.

The Wheeler benchmark problem [2] in Czochralski crystal growth is taken as the test example to validate our new scheme. The numerical results will be compared with available data of Shu et al. [8] using DQ method and Xu et al. [9] using Quick scheme.

2. Wheelers benchmark problem

The Wheeler benchmark problem for Czochralski crystal growth is shown in Fig. 1. It consists of a vertical cylindrical crucible of radius R_c filled with a melt to a height H and rotating with an angular velocity Ω_c. The melt is bounded above by a coaxial crystal of radius $R_x < R_c$ rotating with angular velocity Ω_x.

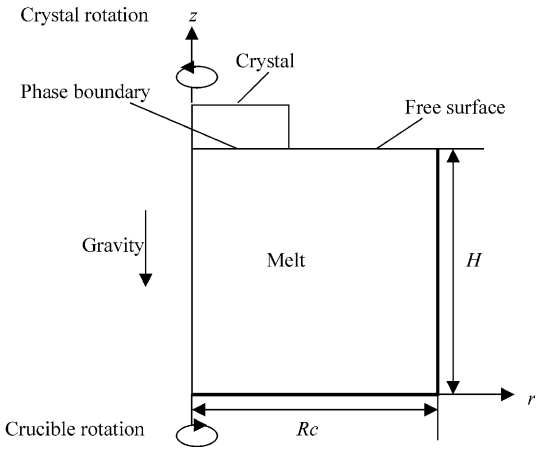

Fig. 1. The configuration of Czochralski crystal growth.

This problem is solved under the assumption that the flow is axisymmetric, so the governing equations in the cylindrical coordinate system can be written as

$$\frac{1}{r}\frac{\partial(ru)}{\partial r}+\frac{\partial w}{\partial z}=0, \tag{1a}$$

$$u\frac{\partial u}{\partial r}+w\frac{\partial u}{\partial z}-\frac{v^2}{r}=-\frac{1}{\rho}\frac{\partial p}{\partial r}+\upsilon\left(\nabla^2 u-\frac{u}{r^2}\right), \tag{1b}$$

$$u\frac{\partial v}{\partial r}+w\frac{\partial v}{\partial z}+\frac{uv}{r}=\upsilon\left(\nabla^2 v-\frac{v}{r^2}\right), \tag{1c}$$

$$u\frac{\partial w}{\partial r}+w\frac{\partial w}{\partial z}=-\frac{1}{\rho}\frac{\partial p}{\partial z}+\upsilon\nabla^2 w+g\beta(T-T_c), \tag{1d}$$

$$u\frac{\partial T}{\partial r}+w\frac{\partial T}{\partial z}=\frac{k}{\rho c_p}\nabla^2 T, \tag{1e}$$

where

$$\nabla^2=\frac{1}{r}\frac{\partial}{\partial r}\left(r\frac{\partial}{\partial r}\right)+\frac{\partial^2}{\partial z^2}.$$

u, v and w are radial, azimuthal and axial velocity components; p is the pressure; T is the temperature; υ is the kinetic viscosity; g is the gravitational acceleration; k is the thermal conductivity; ρ is the density of the melt and c_p is the specific heat at constant pressure.

The boundary conditions for this flow problem are given by

$$u=v=\frac{\partial w}{\partial r}=\frac{\partial T}{\partial r}=0 \qquad \text{for } r=0,\ 0\leqslant z\leqslant\alpha, \tag{2a}$$

$$u=w=0,\quad v=\Omega_c R_c,\quad T=T_c \qquad \text{for } r=1,\ 0\leqslant z\leqslant\alpha, \tag{2b}$$

$$u = w = \frac{\partial T}{\partial z} = 0, \quad v = r\Omega_c R_c \qquad \text{for } z = 0,\ 0 \leqslant r \leqslant 1, \tag{2c}$$

$$\frac{\partial u}{\partial z} = \frac{\partial v}{\partial z} = w = 0, \quad T = T_x + \frac{(r-\beta)}{(1-\beta)}(T_c - T_x) \qquad \text{for } z = \alpha,\ \beta \leqslant r \leqslant 1, \tag{2d}$$

$$u = w = 0, \quad T = T_x, \quad v = r\Omega_x R_x \qquad \text{for } z = \alpha,\ 0 \leqslant r \leqslant \beta, \tag{2e}$$

where

$$\alpha = \frac{H}{R_c}, \quad \beta = \frac{R_x}{R_c}.$$

The non-dimensional parameters: Reynolds numbers, Prandtl and Grashof numbers are defined, respectively, as

$$Re_x = \frac{R_c^2 \Omega_x}{\upsilon}, \quad Re_c = \frac{R_c^2 \Omega_c}{\upsilon}, \quad Pr = \frac{\rho \upsilon c_p}{k}, \quad Gr = \frac{g\beta(T_c - T_x)R_c^3}{\upsilon^2}. \tag{3}$$

In the present study, the aspect ratios and the Prandtl number are fixed at

$$\alpha = 1, \quad \beta = 0.4, \quad Pr = 0.05. \tag{4}$$

3. Mathematical model

3.1. Standard lattice Boltzmann method (LBM)

Using LBM, the continuity and NS equations are not solved directly. Instead, a lattice Boltzmann equation is formulated such that the hydrodynamics satisfies the correct continuity and NS equations by Chapman–Enskog expansion. The flow problem is solved in terms of particle distribution function, f_α. The quantity of $f_\alpha(\boldsymbol{x}, t, \boldsymbol{e})$ relates to the probability of finding a particle in the vicinity of $\boldsymbol{x}$ at time t that is moving with velocity $\boldsymbol{e}_\alpha$. Unlike the continuous particle distribution function in kinetic theory, f_α is defined only for a fixed set of velocities denoted by the subscript α and the lattice model is usually defined on the Cartesian coordinate system. Take the two-dimensional case as an example. The evolution equation for the standard LBM is as follows:

$$f_\alpha\big(x + \delta e_{\alpha x}, y + \delta e_{\alpha y}, t + \delta\big) - f_\alpha(x, y, t) = -\frac{1}{\tau}\big(f_\alpha(x, y, t) - f_\alpha^{\mathrm{eq}}(x, y, t)\big), \tag{5}$$

where τ is the single relaxation time, which characterizes the rate of decay toward equilibrium; f_α is the distribution function along the α direction; f_α^{eq} is its corresponding equilibrium state, which is the distribution to which the system will evolve in the absence of forcing gradients; δ is the time step and $\boldsymbol{e}_\alpha(e_{\alpha x}, e_{\alpha y})$ is the particle velocity in the α direction.

Starting from an initial state, the configuration of particles at each time step evolves in two sequential sub-steps: streaming and collision. During the streaming process, each particle moves to the nearest node in the direction of its velocity, so this process in phase space is linear, which contrasts with the nonlinear convection terms in other approaches that use a macroscopic representation. Obviously, there is no need to do the discretization for this convection term. So the problems caused by the discretization of the convection terms in NS equations can be avoided. Also from this streaming process, we can see the essential

restriction of the standard LBM to the lattice-uniformity. Suppose that a particle is initially at the grid point (x, y, t). Along the α direction, this particle will stream to the position $(x + e_{\alpha x}\delta, y + e_{\alpha y}\delta, t + \delta)$. In the numerical simulation, only the distribution function at the mesh points for all the time levels are needed, so that the macroscopic properties such as the density, flow velocity and temperature can be evaluated at every mesh point. This will require the uniformity of the lattice with $\delta x = e_{\alpha x}\delta, \delta y = e_{\alpha y}\delta$. During the collision process, particles arriving at a node interact and change their velocity directions according to scattering rules. Simple convection combined with a collision process allows the recovery of the nonlinear macroscopic advection through multi-scale expansions.

The macroscopic density ρ and momentum density $\rho \boldsymbol{V}$ are calculated from moments of the particle distribution in direct analogy with the integral moments from kinetic theory. They are defined as

$$\rho = \sum_{\alpha=0}^{N} f_\alpha, \quad \rho \boldsymbol{V} = \sum_{\alpha=0}^{N} f_\alpha \boldsymbol{e}_\alpha. \tag{6}$$

The continuity and NS equations can be recovered by performing a Taylor series expansion of the particle distribution function (5) about the location (x, y) and time t, and a near equilibrium expansion. The detailed information about this process is given by Hou et al. [11]. By doing the above-mentioned Chapman–Enskog expansion, the following equations on Cartesian coordinate system can be recovered:

$$\frac{\partial u}{\partial x} + \frac{\partial v}{\partial y} = 0, \tag{7a}$$

$$\frac{\partial u}{\partial t} + u\frac{\partial u}{\partial x} + v\frac{\partial u}{\partial y} = -\frac{1}{\rho}\frac{\partial p}{\partial x} + \upsilon\nabla^2 u, \tag{7b}$$

$$\frac{\partial v}{\partial t} + u\frac{\partial v}{\partial x} + v\frac{\partial v}{\partial y} = -\frac{1}{\rho}\frac{\partial p}{\partial y} + \upsilon\nabla^2 v. \tag{7c}$$

From Eqs. (7a) and (7b), we can see that the continuity and NS equations recovered by Chapman–Enskog expansion are for the Cartesian coordinate system.

However, the above-mentioned crystal growth flow is an axisymmetric problem defined on the cylindrical coordinate system. If we solve it on the Cartesian coordinate system, we have to solve the real three-dimensional problem using three-dimensional lattice model, which makes the problem more complex as compared with the conventional methods. Furthermore, when the uniform grid is used, the curved boundary cannot be accurately represented. We should find a way to transform the standard LBM to some specific form with which the Chapman–Enskog expansion would recover the continuity and NS equations on the cylindrical coordinate system.

3.2. Axisymmetric lattice Boltzmann model

Since the azimuthal coordinate and its derivatives vanish, there are only two coordinate variables: z and r for an axisymmetric problem. In order to compare the governing equations on the cylindrical coordinate system with those on two-dimensional Cartesian coordinate system, we make the following transformation. By making the replacements $(z, r) \to (y, x)$, $(w, u) \to (v, u)$, $(v) \to (w)$, we can obtain a pseudo-Cartesian representation for Eqs. (1a), (1b) and (1d)

$$\frac{\partial u}{\partial x} + \frac{\partial v}{\partial y} = \underline{-\frac{u}{x}}, \tag{8a}$$

$$\frac{\partial u}{\partial t}+u\frac{\partial u}{\partial x}+v\frac{\partial u}{\partial y}=-\frac{1}{\rho}\frac{\partial p}{\partial x}+\upsilon\nabla^2 u\underline{+\frac{w^2}{x}+\upsilon\left(\frac{1}{x}\frac{\partial u}{\partial x}-\frac{u}{x^2}\right)}, \tag{8b}$$

$$\frac{\partial v}{\partial t}+u\frac{\partial v}{\partial x}+v\frac{\partial v}{\partial y}=-\frac{1}{\rho}\frac{\partial p}{\partial y}+\upsilon\nabla^2 v\underline{+g\beta(T-T_c)}+\upsilon\underline{\left(\frac{1}{x}\frac{\partial v}{\partial x}\right)}, \tag{8c}$$

where

$$\nabla^2=\frac{\partial^2}{\partial x^2}+\frac{\partial^2}{\partial y^2}.$$

Compared with the real governing equations (7a)–(7c) on the Cartesian coordinate system, these equations contain the additional terms which are underlined. We can consider them as the inertia forces from coordinate transformation. As we know, with the Chapman–Enskog expansion, the standard LBM can recover the continuity and NS equations in Cartesian coordinate system. If we consider the underlined terms as the external forces, by inserting the position and time dependent forcing terms into the standard LBM and following the same Chapman–Enskog expansion, we may recover Eqs. (8a)–(8c) by choosing the proper forms of the external forcing terms.

As emphasized in [1], in order to model the departures from the equilibrium in corresponding to the unadjusted LBGK scheme, there is no "equilibrium" for the external forcing terms and these external forcing terms should be at least in $O(\delta)$. Incorporating such time, spatial and particle velocity dependent force terms into the evolution equation of the standard LBM gives

$$f_\alpha(x+\delta e_{\alpha x},y+\delta e_{\alpha y},t+\delta)-f_\alpha(x,y,t)=-\frac{1}{\tau}\left(f_\alpha(x,y,t)-f_\alpha^{eq}(x,y,t)\right)+\delta G+\delta F_1+\delta^2 F_2, \tag{9}$$

where $G=g\beta(T-T_c)\boldsymbol{j}\cdot(\boldsymbol{e}-\boldsymbol{V})f^{eq}$ is used to recover the buoyancy force in the governing equations [12]. Since the form of this force term is known, we only need to consider the force terms of F_1 and F_2.

The Taylor series expansion of Eq. (9) retaining terms up to $O(\delta^2)$ results in

$$\delta[\partial_t+\boldsymbol{e}_\alpha\cdot\nabla]f_\alpha+\frac{\delta^2}{2}[\partial_t+\boldsymbol{e}_\alpha\cdot\nabla]^2 f_\alpha+O(\delta^3)=-\frac{1}{\tau}\left(f_\alpha-f_\alpha^{eq}\right)+\delta F_1+\delta^2 F_2. \tag{10}$$

The Chapman–Enskog expansion of the above Taylor expanded evolution equation plus the force terms at $O(\delta)$ and $O(\delta^2)$ are

$$\left(\partial_{t0}+e_{\alpha\gamma}\partial_\gamma\right)f_\alpha^{eq}=-\frac{1}{\tau}f_\alpha^{(1)}+F_1, \tag{11a}$$

$$\partial_{t1}f_\alpha^{eq}+\left(1-\frac{1}{2\tau}\right)(\partial_{t0}+\boldsymbol{e}_\alpha\cdot\nabla)f_\alpha^{(1)}+\frac{1}{2}(\partial_{t0}+\boldsymbol{e}_\alpha\cdot\nabla)F_1=-\frac{1}{\tau}f_\alpha^{(2)}+F_2. \tag{11b}$$

The summation of Eq. (11a) and the summation of Eq. (11a) multiplied by $\boldsymbol{e}_\alpha$ give the continuity and Euler equations

$$\partial_{t0}\rho+\nabla\cdot(\rho\boldsymbol{V})=\sum_\alpha F_1, \tag{12a}$$

$$\partial_{t0}(\rho\boldsymbol{V})+\nabla\cdot\Pi^{(0)}=\sum_\alpha F_1\boldsymbol{e}_\alpha, \tag{12b}$$

where $\Pi^{(0)}=\sum_\alpha \boldsymbol{e}_\alpha\boldsymbol{e}_\alpha f_\alpha^{eq}$.

Compared with the convection part of Eqs. (8a)–(8c), we can get

$$\sum_{\alpha} F_1 = \frac{-\rho u}{x}, \tag{13a}$$

$$\sum_{\alpha} F_1 e_{\alpha\gamma} = \frac{\rho w^2}{x}\delta_{\gamma x}. \tag{13b}$$

The summation of Eq. (11b) and the summation of Eq. (11b) multiplied by $\boldsymbol{e}_\alpha$ are

$$\partial_{t1}\rho + \frac{1}{2}\partial_{t0}\left(\sum_{\alpha} F_1\right) + \frac{1}{2}\nabla\cdot\left(\sum_{\alpha} F_1 \boldsymbol{e}_\alpha\right) = \sum_{\alpha} F_2, \tag{14a}$$

$$\partial_{t1}(\rho \boldsymbol{V}) + \left(1 - \frac{1}{2\tau}\right)\nabla\cdot\Pi^{(1)} + \frac{1}{2}\partial_{t0}\left(\sum_{\alpha} \boldsymbol{e}_\alpha F_1\right) + \frac{1}{2}\nabla\cdot\left(\boldsymbol{e}_\alpha \boldsymbol{e}_\alpha F_1\right) = \sum_{\alpha} F_2 \boldsymbol{e}_\alpha, \tag{14b}$$

where $\Pi^{(1)} = \sum_\alpha \boldsymbol{e}_\alpha \boldsymbol{e}_\alpha f_\alpha^{(1)}$.

Eq. (14a) plus (12a) and (14b) plus (12b) should recover the continuity and NS Eqs. (8a)–(8c). So the following relationships should be satisfied:

$$\sum_{\alpha} F_2 = \frac{1}{2x}\left[\partial_x(\rho u^2) + \partial_y(\rho u v) + \partial_x(p) + \partial_x(\rho w^2) - \frac{2\rho w^2}{x}\right], \tag{15a}$$

$$\sum_{\alpha} F_2 e_{\alpha x} = -\frac{w}{x}\left[\partial_x(\rho u w) + \partial_y(\rho v w) + \frac{\rho u w}{x}\right] - \frac{1}{6x}\partial_x(\rho u) + \frac{\rho u}{6x^2}, \tag{15b}$$

$$\sum_{\alpha} F_2 e_{\alpha y} = -\frac{1}{6x}\partial_y(\rho u) + \frac{v}{x}\left[\partial_x(\rho v) - \partial_y(\rho u)\right]. \tag{15c}$$

During the derivation, the 9-bit particle model defined as

$$\boldsymbol{e}_\alpha = \begin{cases} 0, & \alpha = 0, \\ (\cos[(\alpha-1)\pi/2], \sin[(\alpha-1)\pi/2])c, & \alpha = 1,2,3,4, \\ \sqrt{2}\left(\cos[(\alpha-5)\pi/2+\pi/4], \sin\left[\left(\alpha-5\right)\pi/2+\pi/4\right]\right)c, & \alpha = 5,6,7,8, \end{cases}$$

is used, whose equilibrium distribution can be written as

$$f_\alpha^{\mathrm{eq}} = t_p\rho\left[1 + \frac{3\boldsymbol{e}_\alpha\cdot\boldsymbol{V}}{c^2} + \frac{9(\boldsymbol{e}_\alpha\cdot\boldsymbol{V})^2}{2c^4} - \frac{3\boldsymbol{V}^2}{2c^2}\right], \tag{16}$$

where $t_p = 4/9$ for $\alpha = 0$; $t_p = 1/9$ for $\alpha = 1,2,3,4$; and $t_p = 1/36$ for $\alpha = 5,6,7,8$.

The final forms of the external forces can be represented as

$$F_1 = t_p\left(F_{10} + 3F_{11}e_{\alpha x} + 3F_{12}e_{\alpha y}\right), \tag{17a}$$

where $F_{10} = -\rho u/x$, $F_{11} = \rho w^2/x$, $F_{12} = 0$;

$$F_2 = t_p\left(F_{20} + 3F_{21}e_{\alpha x} + 3F_{22}e_{\alpha y}\right), \tag{17b}$$

where

$$F_{20} = \frac{1}{2x}\left[\partial_x\left(\rho u^2\right) + \partial_y(\rho uv) + \partial_x p + \partial_x\left(\rho w^2\right) - \frac{2\rho w^2}{x}\right],$$

$$F_{21} = -\frac{w}{x}\left[\partial_x(\rho uw) + \partial_y(\rho vw) + \frac{\rho uw}{x}\right] - \frac{1}{6x}\partial_x(\rho u) + \frac{\rho u}{6x^2},$$

$$F_{22} = -\frac{1}{6x}\partial_y(\rho u) + \frac{\upsilon}{x}\left[\partial_x(\rho v) - \partial_y(\rho u)\right].$$

By adding these force terms to the standard LBM, the governing Eqs. (8a)–(8c), which are the same as Eqs. (1a), (1b) and (1d), can be correctly recovered on the cylindrical coordinate system by Chapman–Enskog expansion.

Note that the form of the source terms is not unique. During the above derivation, F_1 and F_2 are determined independently. The form of F_1 can be used explicitly to determine an appropriate form for F_2. It can be seen clearly that Eqs. (8a)–(8c) and (17a), (17b) have singularity at $x = 0$, which is the axisymmetric line for the problem. Fortunately, this difficulty can be easily overcome by streaming process and implementing the axisymmetric boundary condition at $x = 0$. In other words, Eqs. (8a)–(8c) and (17a), (17b) are only applied at position of $x \neq 0$.

Although the explicit inclusion of gradients to the standard LBM undermines the simple formulation of the standard LBM, these terms are necessary to recover their target dynamics and the discretization scheme of these gradients has no effect on the stability of the scheme itself. We can just use the simple central difference scheme to do numerical discretization.

The azimuthal velocity and the temperature are obtained through the following equations by using first-order forward difference scheme in time and second-order central difference scheme in space:

$$\frac{\partial w}{\partial t} + u\frac{\partial w}{\partial x} + v\frac{\partial w}{\partial y} + \frac{uw}{x} = \upsilon\left(\nabla^2 w + \frac{1}{x}\frac{\partial w}{\partial x} - \frac{w}{x^2}\right), \tag{18a}$$

$$\frac{\partial T}{\partial t} + u\frac{\partial T}{\partial x} + v\frac{\partial T}{\partial y} = \frac{k}{\rho c_p}\left(\nabla^2 T + \frac{1}{x}\frac{\partial T}{\partial x}\right), \tag{18b}$$

where

$$\nabla^2 = \frac{\partial^2}{\partial x^2} + \frac{\partial^2}{\partial y^2}.$$

From the above derivation, it can be seen that after such transformation, the axisymmetric flow problem on the cylindrical coordinate system can be solved on a uniform rectangular two-dimensional grid, which adheres to the inherit property, lattice-uniformity, of LBM. The curved boundary can be well defined using uniform rectangular grid. At the same time, it also avoids the solution of the real three-dimensional problem on Cartesian coordinate system for such quasi-three-dimensional flow problem.

4. Non-dimensional parameters and boundary conditions

The system is normalized in the following way: the characteristic length is R_c; the characteristic velocity is $c = \delta x/\delta t$. The non-dimensional temperature is $T' = (T - T_x)/(T_c - T_x)$.

The non-dimensional parameter τ in Eq. (9) is determined by its relationship with the non-dimensional kinetic viscosity $\tau = (3\upsilon')/\delta t + 0.5$. When the Reynolds number R_x is given, the non-dimensional kinetic viscosity is obtained by $\upsilon' = v_x/(Re_x\beta)$; when the Gr is given, the non-dimensional kinetic viscosity is obtained by $\upsilon' = v_h/\sqrt{Gr}$. v_x and $v_h = \sqrt{\beta g \Delta T R_c}$ are the non-dimensional velocity for the crystal at $x = R_x$ and the non-dimensional characteristic velocity for the natural convection problem, respectively. To ensure the code working properly in the near-incompressible regime, we carefully choose the value of v_x and v_h. They are required to be less than 0.3. In the present study, they are chosen to be 0.1 at low Reynolds or Grashof number and be 0.15 at high Reynolds or Grashof number.

The implementation of boundary condition is very important in the simulation. The unknown distribution functions pointing into the fluid field at the boundary node must be specified. There are three different kinds of boundary conditions in the Czochralski flow: the axisymmetric boundary condition, the wall boundary condition and the free surface condition. For different boundary condition, the unknown distribution functions have different relationship with the known distribution functions. Fig. 2 shows the configuration of particle velocity directions at four boundaries.

For $x = 0$, $0 \leqslant y \leqslant \alpha$, this is the axisymmetric boundary and the specular boundary condition is used. After streaming process, the distributions at directions 2, 3, 4, 6, 7 are known which are determined by Eq. (9). The unknown distributions at directions 1, 5, 8 can be determined from the following boundary conditions:

$$f_1 = f_3, \quad f_5 = f_6, \quad f_8 = f_7. \tag{19a}$$

For $x = 1$, $0 \leqslant z \leqslant \alpha$, this is the wall boundary and the bounce back condition of the non-equilibrium distribution is used [13]. After streaming process, the distributions at directions 1, 2, 4, 5, 8 are known and the unknown distributions at directions 3, 6, 7 can be determined from the following boundary conditions:

$$f_3 = f_3^{eq} + f_1 - f_1^{eq}, \quad f_6 = f_6^{eq} + f_8 - f_8^{eq}, \quad f_7 = f_7^{eq} + f_5 - f_5^{eq}. \tag{19b}$$

For $z = 0$, $0 \leqslant x \leqslant 1$, this is also the wall boundary and the bounce back condition of the non-equilibrium distribution is used. After streaming process, the distributions at directions 1, 3, 4, 7, 8 are known and the unknown distributions at directions 2, 5, 6 can be determined from the following boundary conditions:

$$f_2 = f_2^{eq} + f_4 - f_4^{eq}, \quad f_5 = f_5^{eq} + f_7 - f_7^{eq}, \quad f_6 = f_6^{eq} + f_8 - f_8^{eq}. \tag{19c}$$

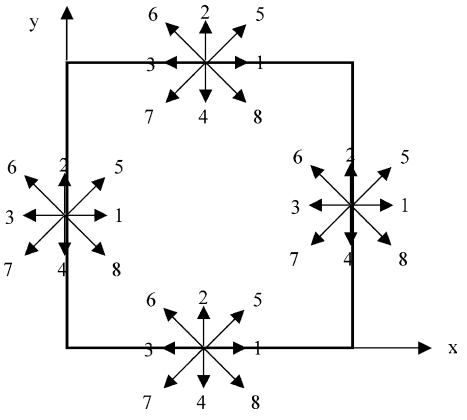

Fig. 2. Schematic plots of velocity directions at boundaries.

For $z = \alpha$, $\beta \leqslant x \leqslant 1$, this is the free surface and the specular boundary condition is used. After streaming process, the distributions at directions 1, 2, 3, 5, 6 are known and the unknown distributions at directions 4, 7, 8 can be determined from the following boundary conditions:

$$f_4 = f_2, \quad f_7 = f_6, \quad f_8 = f_5. \tag{19d}$$

For $z = \alpha$, $0 \leqslant x \leqslant \beta$, we consider it as the wall boundary and the bounce back condition of the non-equilibrium distribution is used. After streaming process, the distributions at directions 1, 2, 3, 5, 6 are known and the unknown distributions at directions 4, 7, 8 can be determined from the following boundary conditions:

$$f_4 = f_4^{\mathrm{eq}} + f_2 - f_2^{\mathrm{eq}}, \quad f_7 = f_7^{\mathrm{eq}} + f_5 - f_5^{\mathrm{eq}}, \quad f_8 = f_8^{\mathrm{eq}} + f_6 - f_6^{\mathrm{eq}}. \tag{19e}$$

5. Results and discussion

To validate the new scheme, the numerical simulation of Wheeler's problem is chosen as a test case. In this study, we firstly study how the forced convection and natural convection affect the flow fields differently. So we consider the following three cases A1, B1 and C1, which are defined as

$$\text{A1}: \ Re_x = 100., \ Re_{\mathrm{c}} = 0., \ Gr = 0,$$

$$\text{B1}: \ Re_x = 100., \ Re_{\mathrm{c}} = -25.0, \ Gr = 0,$$

$$\text{C1}: \ Re_x = 0., \ Re_{\mathrm{c}} = 0., \ Gr = 10^5.$$

Cases A1 and B1 are forced convection problems caused by different mechanics. The flow in Case A1 is driven by the rotation of the crystal, while the flow in Case B1 is generated by opposite rotations of the crystal and the crucible. Case C1 is a natural convection problem.

The mesh size used for these three cases is 101×101. The convergence criterion for all the cases is set to

$$\max \sum_{i,j} \left| \sqrt{(u_{i,j}^2 + v_{i,j}^2)^{n+1}} - \sqrt{(u_{i,j}^2 + v_{i,j}^2)^{n}} \right| \leqslant 10^{-8}$$

and

$$\max \sum_{i,j} \left| w^{n+1} - w^n \right| \leqslant 10^{-8}, \quad \max \sum_{i,j} \left| T^{n+1} - T^n \right| \leqslant 10^{-8},$$

where n and $n+1$ represent the old and new time levels, respectively.

Table 1 shows the comparison of computed minimum and maximum stream functions for these three cases with benchmark results. The stream function is computed through

Table 1
Comparison of computed minimum and maximum stream function for Cases A1, B1 and C1

Case	Gr	Re_x	Re_{c}	$\psi_{\min}$ (present)	$\psi_{\max}$ (present)	$\psi_{\min}$ (DQ [8])	$\psi_{\max}$ (DQ [8])
A1	0.	10^2	0.	−0.221	5.46×10^{-6}	−0.222	5.46×10^{-6}
B1	0.	10^2	−25.	-5.14×10^{-2}	0.114	-6.81×10^{-2}	0.117
C1	10^5	0.	0.	-5.18×10^{-3}	29.884	-7.50×10^{-3}	28.316

$$\frac{\partial \psi}{\partial x} = -xv, \quad \frac{\partial \psi}{\partial y} = xu. \tag{20}$$

From Table 1, we can see that the maximum absolute value of stream function for each case agrees very well with that computed by the DQ method [8], and the maximum difference is within 3%. There are some deviations between the computed minimum absolute values of stream function. These deviations can be considered to be negligible since the minimum absolute values are very small. The streamlines and isotherms for Cases A1, B1 and C1 are shown in Figs. 3–5.

Although the streamlines are quite different for Cases A1 and B1, the contours of temperature are very similar. This indicates the similarity of the temperature fields for forced convection problems. On the contrary, the temperature field for the Case C1 is quite different from Cases A1 and B1, and this shows the effect of buoyancy force on the temperature field.

Since the natural convection has been well studied, while the forced convections draw less attention as compared with the natural convection, we put the emphasis on the forced convection in the following study. We study the influence of the rotations of the crystal and crucible on the forced convection problems, and two more cases which have different rotation velocities are studied. They are defined as

$$\text{A2}: \ Re_x = 1000, \ Re_c = 0, \ Gr = 0,$$

$$\text{B2}: \ Re_x = 1000, \ Re_c = -250, \ Gr = 0.$$

The mesh size used for the study is 201×201.

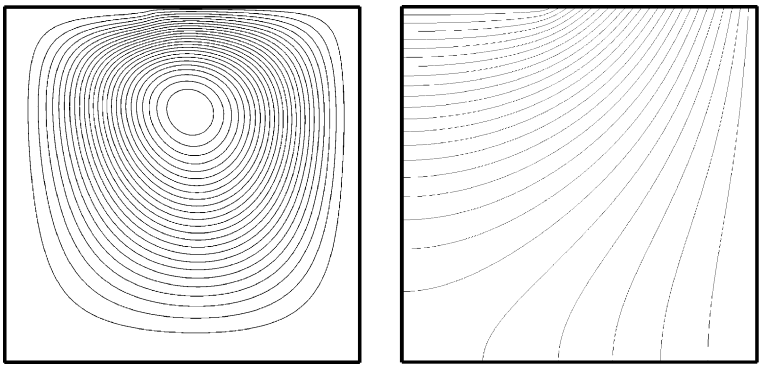

Fig. 3. Streamline and temperature contour of Case A1.

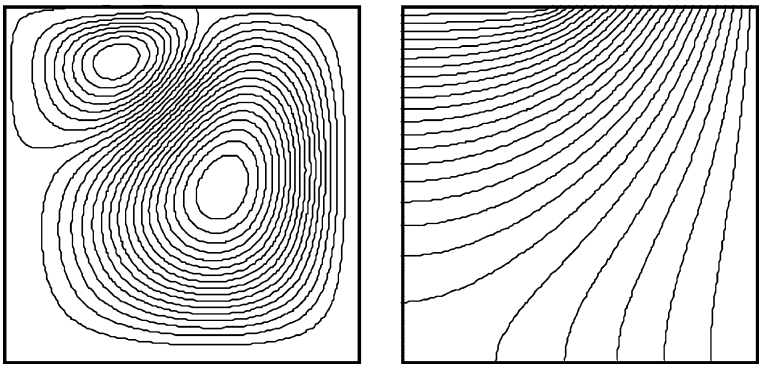

Fig. 4. Streamline and temperature contour of Case B1.

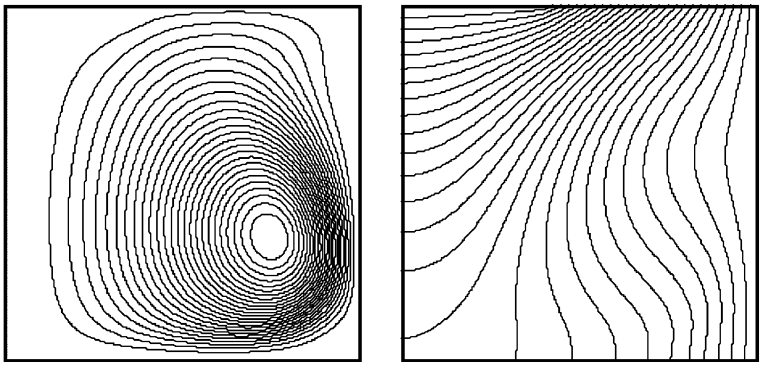

Fig. 5. Streamline and temperature contour of Case C1.

Table 2
Comparison of computed minimum and maximum stream function for Cases A1, A2, B1 and B2

Case	Gr	Re_x	Re_c	ψ_{min} (present)	ψ_{max} (present)	ψ_{min} (quick [9])	ψ_{max} (quick [9])
A1	0.	10^2	0.	−0.221	5.46×10^{-6}	−0.217	4.06×10^{-6}
A2	0.	10^3	0.	−5.075	1.06×10^{-4}	−4.994	1.83×10^{-5}
B1	0.	10^2	−25.	-5.14×10^{-2}	0.114	-4.43×10^{-2}	0.117
B2	0.	10^3	−250.	−1.478	1.114	−1.478	1.148

Table 2 shows the comparison of computed minimum and maximum stream functions at different rotations. The benchmark results using Quick scheme [9] are also included for validation.

From Table 2, we can see that the maximum absolute value of stream function for each case agrees very well with the benchmark results.

For the Case A2, it can be seen from Table 2 that the absolute value of the stream function increases with the increase of the rotation velocity, which means that the intensity of the vortex increases. The maximum absolute stream function increases from 0.221 to 5.0575 when the rotation velocity increases from 10^2 to 10^3. The streamlines and temperature contours are similar to Case A1, which will not be repeated. The only difference for the streamlines is that the center of the vortex induced by the rotation moves towards the sidewall of the crucible and is deformed increasingly. The highest velocity region moves from the upper left corner to the upper right corner. This shows that with the increase of the rotation velocity, better quality crystal can be produced.

For the Case B2, it can be seen from Table 2 that the absolute value of the stream function also increases with the increase of the rotation velocity. The streamlines and temperature contours are also similar to Case B1. It can be seen from the streamlines that there are two vortices with opposite directions appearing in the upper left corner just under the crystal and the lower right corner. This means that the rotations of both crystal and crucible cannot produce good quality of crystal. With increase of the rotational speeds of the crystal and crucible, the upper left vortex will move to the right corner, and the lower vortex will move to the left and dominate the flow field.

6. Conclusions

The application of the new scheme to simulate the flow in Czochralski crystal growth demonstrates that our new scheme could solve the axisymmetric thermal problem effectively. The numerical results compare

well with those from NS solvers, and show that LBM provides a completely different way to solve the crystal growth problem. It is worth to mention that our new scheme can solve the axisymmetric flow problem on a uniform rectangular two-dimensional grid in the cylindrical coordinate system, avoiding the solution of the real three-dimensional problem on Cartesian coordinate system if using the standard LBM.

References

[1] I. Halliday, L.A. Hammond, C.M. Care, K. Good, A. Stevens, Phys. Rev. E 64 (2001) 011208.
[2] A.A. Wheeler, J. Crystal Growth 102 (1990) 691.
[3] W.E. Langlois, Annu. Rev. Fluid Mech. 17 (1985) 191.
[4] U. Buckle, M. Schafer, J. Crystal Growth 126 (1993) 682.
[5] J.R. Ristorcelli, J.L. Lumley, J. Crystal Growth 129 (1993) 249.
[6] Q. Xiao, J.J. Derby, J. Crystal Growth 139 (1994) 147.
[7] I. Paspo, J. Ouazzani, R. Peyret, Int. J. Numer. Methods Heat Fluid Flow 6 (1996) 31.
[8] C. Shu, Y.T. Chew, Y. Liu, J. Crystal Growth 181 (1997) 427.
[9] D. Xu, C. Shu, B.C. Khoo, J. Crystal Growth 173 (1997) 123.
[10] S. Chen, D.D. Gary, Annu. Rev. Fluid Mech. 30 (1998) 329.
[11] S. Hou, Q. Zou, S. Chen, G.D. Doolen, A.C. Cogley, J. Comput. Phys. 118 (1995) 329.
[12] X. He, S. Chen, D.D. Gary, J. Comput. Phys. 146 (1998) 282.
[13] Q. Zou, X. He, Phys. Fluids 9 (1997) 1591.